Modification of thermal transport in an individual carbon nanofiber by focused ion beam irradiation

Narasaki, Masahiro
Department of Aeronautics and Astronautics, Kyushu University

Li, Qin-Yi
Department of Aeronautics and Astronautics, Kyushu University

Ikuta, Tatsuya
Department of Aeronautics and Astronautics, Kyushu University

Miyawaki, Jin
Institute for Materials Chemistry and Engineering, Kyushu University

他

https://hdl.handle.net/2324/7162464

出版情報：Carbon. 153, pp.539-544, 2019-11. Elsevier
バージョン：
権利関係：

Modification of thermal transport in an individual carbon nanofiber by focused ion beam irradiation

Masahiro Narasaki,[a, b] Qin-Yi Li, [a, b] Tatsuya Ikuta,[a, b] Jin Miyawaki,[c] and Koji Takahashi[a, b, *]

[a] Department of Aeronautics and Astronautics, Kyushu University, 744 Motooka, Fukuoka 819-0395, Japan

[b] International Institute for Carbon-Neutral Energy Research (WPI-I2CNER), Kyushu University, 744 Motooka, Fukuoka 819-0395, Japan

[c] Institute for Materials Chemistry and Engineering, Kyushu University, 6-1 Kasugakoen, Kasuga-shi, Fukuoka 816-8580, Japan

Abstract

We report on the in situ thermal measurement of a carbon nanofiber (CNF) modified by focused ion beam (FIB) irradiation. The FIB irradiation led to local amorphization of the crystalline structure of the CNF. The in situ measurement was improved by correcting for the effect of the scattered ions on the sensor. The low effective thermal conductivity of the pristine CNF (~39 W/mK) resulted from the anisotropic structure made of many individual graphitic fibers. The first FIB irradiation decreased the thermal conductivity by approximately 3.2%. This relatively small decrease is attributed to the structure of the CNF consisting of many individual fibers, with some fibers remaining pristine even after the FIB irradiation. Analysis using a thermal-circuit model suggested that the thermal transport in the CNF could include a ballistic feature of phonons in the micrometer range. Our proposed in situ thermal measurement method can be extended to the study of thermal transport in various structurally modified nanomaterials.

---

[*] Corresponding author. Tel: +81-92-802-3015. E-mail: takahashi@aero.kyushu-u.ac.jp (Koji Takahashi)

1. Introduction

Graphene-based nanocarbon materials such as carbon nanotubes (CNTs) and graphene have received considerable attention because of their high thermal conductivity [1–6], which is useful for thermal management [7–9]. The high thermal conductivity results from the light carbon atoms and strong *sp*^{2} bonding between atoms. Manipulation of the thermal transport in graphene-based nanocarbon materials has also been achieved by modifying the structures using focused ion beam (FIB) irradiation [10,11], electron beam (EB) irradiation [12], EB-induced deposition [13], fullerene encapsulation [14] and chemical functionalization

[15,16]. These studies highlighted the potential applications of graphene-based nanocarbon materials such as for thermal rectification [13] and thermal conversion [14] and provided estimates of the effects of defects [10,11] and impurities [15,16] on the thermal transport. Nevertheless, experimental studies on the effects of structural modification on thermal transport remain limited as it is difficult to combine thermal measurements and structural modification techniques at the nanoscale. With the acceleration of theoretical studies on phonon engineering, more rigorous experimental methods should also be developed.

Raman spectroscopes or metallic thin-film sensors have conventionally been used for thermal measurement of nanocarbon materials[1,2,5,15,17,18]. Although Raman thermometry requires a relatively brief sample fabrication process, this technique may introduce unexpected error in the measurement results because of the use of laser absorptivity. The preparation of metallic thin-film sensors requires more complicated microelectromechanical system (MEMS) techniques but can result in higher temperature sensitivity because much smaller temperature differences can be detected using the electrical resistances instead of the peak shifts of Raman spectra. The higher temperature sensitivity is important to precisely investigate the effects of structural modification on thermal transport.

In situ thermal measurement of nanomaterials modified by FIB or EB irradiation can be used to study nanomaterials with local structural modification. By using only one sample, this method eliminates the problem of individual differences among samples, which can lead to undesirable deviations in the measured results. FIB irradiation is a better choice than EB irradiation to modify multi-walled carbon nanotubes (MWCNTs) or carbon nanofibers (CNFs), which contain more atoms and are thicker than single-walled carbon nanotubes (SWCNTs) and single-layer graphene (SLG). It is easier to modify these structures using FIB irradiation because the ions are larger than electrons, leading to much faster collapse of the crystalline structures. One concern about using FIB irradiation is the need to account for the effect of the widely scattered ions on the delicate sensors [19–21].

In this work, we performed in situ measurements of the thermal resistance of a graphene-based one-dimensional nanocarbon material, which is a CNF, modified by FIB irradiation using a platinum thin-film sensor. The CNF sample was irradiated with a FIB to adjust the characteristic length of phonon transport down to 1 μm. The thermal conductivity of the pristine CNF was approximately 39 W/mK and decreased by approximately 3.2% after the first FIB irradiation. This low intrinsic thermal conductivity resulted from the anisotropic structure consisting of many individual graphitic fibers. The relatively small decrease is attributed to the structure being composed of many individual graphene-based fibers, with some fibers retaining their crystalline structure even after the FIB irradiation. Analysis using a thermal-circuit model suggested that ballistic phonon transport occurs in the CNF, which can be attributed to the highly graphitized structure of the CNF. This work is useful for understanding ballistic phonon transport and provides knowledge for tailoring the heat flow in nanocarbon materials.

2. Experimental

This investigation involved the preparation of a CNF sample and sensor for measurement, observation of the structure of the CNF using transmission electron microscopy (TEM), characterization of the structure using Raman spectroscopy, measurement of the thermal conductivity of a Pt hot film affected by scattered ions (supplementary material), and in situ measurement of the thermal resistance of the CNF under FIB irradiation.

2.1. *Sample and sensor preparation*

CNF was produced from polyacrylonitrile (PAN) nanofiber as follows. Firstly, PAN nanofiber was prepared by electrospinning method with 8 wt.% PAN/dimethylformamide solution at room temperature using a commercial electrospinning apparatus (NANON, MECC, Co. Ltd., Japan) at 30 kV of applied voltage. Next, to conserve the fibrous structure, the PAN nanofiber was stabilized under air atmosphere from room temperature to 270 °C at 0.5 °C/min of heating rate. The stabilized PAN nanofiber was then carbonized at 600 °C for 1 h in Ar gas flow (heating rate: 5 °C/min). Finally, the carbonized PAN nanofiber was heat-treated at 2800 °C for 10 min to obtain graphitized CNF. The average diameter was 266 nm. The CNF was then ultrasonically dispersed in ethanol solution to isolate the fibers. A

MEMS technique was used to fabricate the Pt thin-film sensors. EB lithography was used to pattern an EB resist layer on a SiO_2/Si substrate. An 8-nm-thick Ti and a 40-nm-thick Pt layer were deposited on the substrate using physical vapor deposition (PVD). After the subsequent lift-off process and wet etching using buffered hydrofluoric solution, the sensor fabrication was completed. The sensor consisted of two Pt electrodes and heat sinks, a Pt hot film suspended between them, and another Pt heat sink. The hot film, which served as a resistance thermometer, was approximately 9.6-μm long, 500-nm wide, and 40-nm thick. After calibration of the Pt hot film, a CNF dispersed on a TEM grid was picked up by a sharpened tungsten probe and bridged between the hot film and heat sink of the sensor. To minimize the thermal contact resistance between the Pt hot film and sample, amorphous carbon was deposited on both ends of the sample [1,2,18,22,23]. Fig. 1 presents a scanning electron microscopy (SEM) image of the sensor and CNF. The slight curvature on the sensor would not affect the measurement because the slight curvature does not break any crystalline structures.

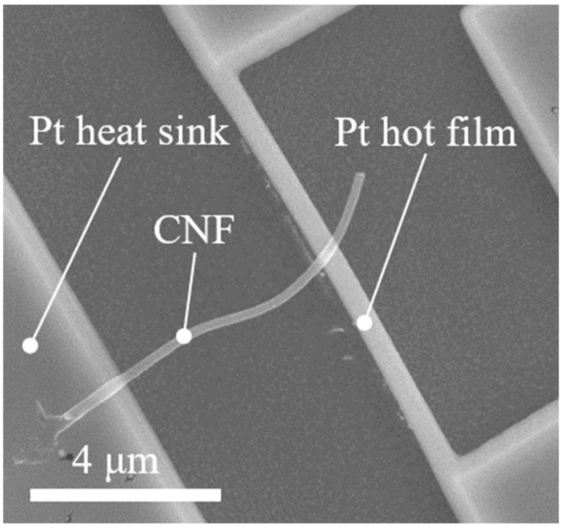

Fig. 1 SEM image of Pt thin-film sensor and CNF bridged between the hot film and heat sink. The Pt hot film and CNF were completely suspended above the SiO_2/Si substrate.

2.2. *TEM observation*

The CNF used for the measurement was examined using TEM (JEM-3200FSK, JEOL Ltd., Japan) to confirm that there were no visible contaminants or defects. Fig. 2 presents a TEM image of an outer edge of the electrospun CNF. More TEM images of the pristine CNFs are in the supplementary material. The TEM images revealed many individual fibers were intertwined to create the CNFs and the fibers were made of the graphitic structure. The graphitic structures were roughly oriented in the axial direction of the CNF and continued essentially in the axial direction. Some fibers went beneath others and/or were twisted. Next, the effects of FIB irradiation on the CNF were verified using another CNF. The crystalline structure was transformed into an amorphous structure by the FIB irradiation. Fig. 3(a) presents a schematic illustration of the FIB irradiation of the CNF. The acceleration voltage, diameter, irradiation area, beam current, and dose were 30 kV, 7.1 nm, 0.1×20 μm^2, 1.6 pA, and 10 pC/μm^2, respectively. Fig. 3(b) presents a TEM image of the FIB-irradiated CNF. We identified the defected parts in the CNF by finding the boundaries between the crystalline and amorphous regions (Fig. S6). The defected part in the CNF was approximately 222-nm long along the fiber axis and occupied approximately 54% of the original cross-section, which was estimated geometrically, as explained in the supplementary material.

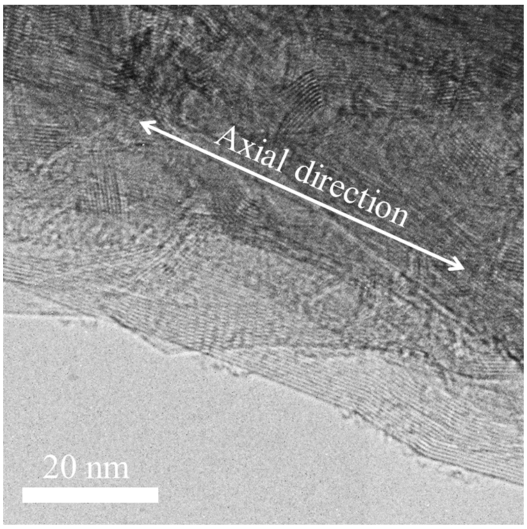

Fig. 2 TEM image of an outer edge of the electrospun CNF. The CNF exhibited a fibrous structure of many individual components of the graphitic structure. More TEM images of the pristine CNFs are in the supplementary material.

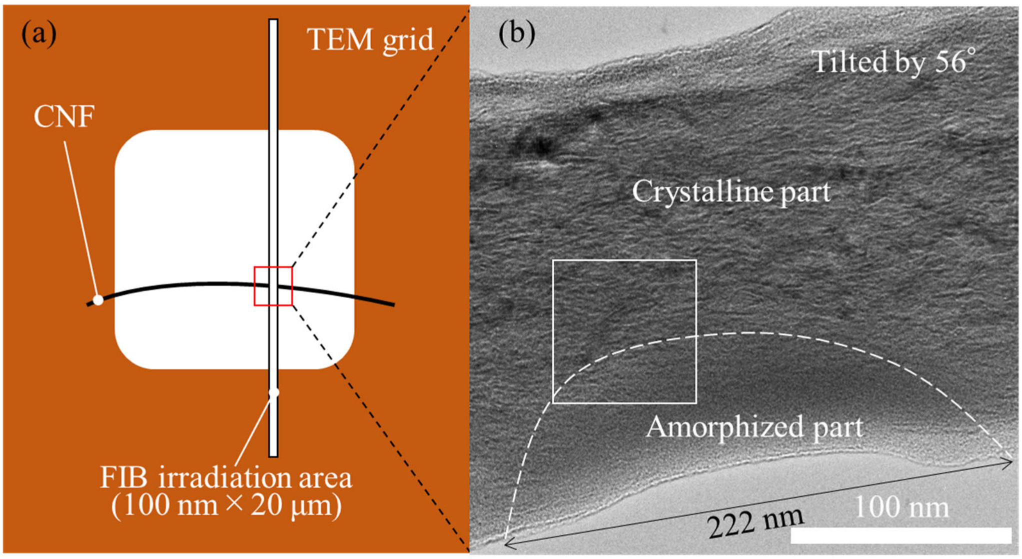

Fig. 3 (a) Schematic illustration of CNF on a TEM grid and FIB irradiation area. (b) TEM image of FIB-irradiated CNF (tilted by 56°). After FIB irradiation, the original structure of the CNF based on the graphitic structure collapsed. The dashed line represents the approximate boundary between the crystalline and amorphized part when the TEM grid was tilted by 56°. The white rectangle in (b) is the approximate area of the boundary between the crystalline and amorphized part shown in Fig. S6.

2.3. *Raman spectroscopy*

Fig. 4 shows a Raman spectrum of the CNF measured by a commercial Raman spectrometer (LabRAM HR-800, Horiba Ltd., Japan). The Raman spectrum shows the two characteristic peaks of graphitic materials. One is D peak (~1370 cm-1) which is associated with the disordered graphitic structure, and the other is G peak (~1590 cm-1) which is associated with sp^2 bonding between carbon atoms in the graphitic structure. The ratio of the intensity of D peak to intensity of G peak indicates how crystalline the graphitic samples are. The intensity ratio of our CNF is much smaller than the other CNFs in the reference [24]. In the reference, the ratio decreased with increase of the final carbonization temperature from 1400 to 2200 °C, indicating more ordered graphitic structures are made. Since we heat-treated the CNF at 2800 °C, the Raman spectrum shows the further smaller ratio. Thus, the CNF used in this study is made of highly crystalline graphitic structure.

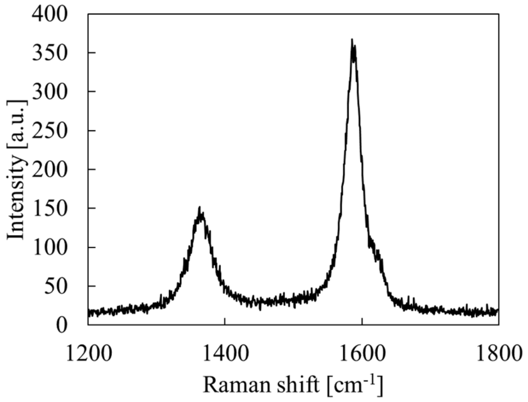

Fig. 4 Raman spectrum of the CNF.

2.4. *Thermal measurement*

Thermal measurement using a T-type method was performed on a Peltier heating/cooling stage in the chamber of a scanning electron microscope (Versa 3D, FEI, OR, USA) equipped with a FIB system. The pressure in the chamber during the measurements was on the order of 10^{-4} Pa. Fig. 4 presents a schematic illustration of the T-type method. In this method, a hot film is heated by a direct current, and the average temperature of the hot film is measured as the electrical resistance. If the hot film is bare, the temperature distribution along the hot film is similar to that indicated by the solid blue line. When a CNF is on the hot film, the temperature distribution is similar to that indicated by the dashed red line because some heat generated in the hot film can escape through the CNF to another heat sink. The difference between the two average temperatures corresponds to the thermal resistance of the CNF. In the experiment, the hot film was first calibrated; then, a CNF was placed on the sensor using a probe; and finally, the thermal resistance of the pristine CNF was measured. The suspended length of the CNF was 5.0 μm, and the diameter was 193 nm. The CNF was irradiated with the first FIB at a position 1-μm away from the hot film. For the following irradiations, the position of the FIB-irradiated area was shifted by 1 μm in the direction away from the hot film, as shown in Fig. 4. After every FIB irradiation, the thermal resistance of the CNF was measured. The effect of the scattered ions on the thermal conductivity of the Pt hot film was corrected to improve the in situ measurement, as explained in the supplementary material.

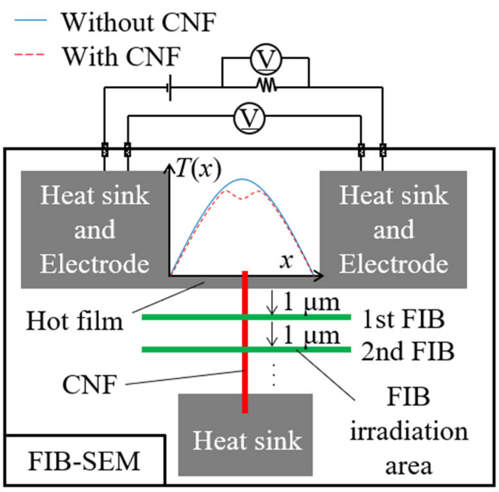

Fig. 4. Schematic illustration of thermal measurement using T-type method.

3. Results and Discussion

The thermal resistances of the CNF at 300 K after the *n*th FIB irradiation are shown in Fig. 5. The thermal resistance of the CNF increased monotonically as the FIB was irradiated. This is attributed to the FIB irradiation collapsed the crystalline structure of the CNF, leading to scatter phonons and shorten the mean free paths. The thermal resistance was converted to the effective thermal conductivity by considering the length (5.0 µm) and diameter (193 nm). The effective thermal conductivity of the pristine CNF was 39 W/mK. The thermal conductivity after the first FIB irradiation decreased by 3.2% compared with the original thermal conductivity.

The effective thermal conductivity of the CNF before the FIB irradiations is lower than the thermal conductivities of SWCNTs (600–10000 W/mK) [3,25–27] and MWCNTs (100–3000

W/mK) [1,2,4,26,28–30]. This lower effective thermal conductivity can be attributed to two anisotropies: the interlayers of the graphitic structures and the gaps between each fiber (Fig. S5). The two isotropies lead to thermal resistances respectively. Fujii et al. reported that the thermal conductivity of a MWCNT decreased with increasing diameter [2], and the same trend was also reported by Yang et al. [29]. Hayashi et al. showed that the thermal conductivity in the radial direction of a MWCNT is much lower than that in the axial direction because of the anisotropic structure of MWCNTs [31]. The inner layers of a MWCNT do not relatively contribute to the thermal conductivity of the axial direction, resulting in the lower effective thermal conductivities of thicker MWCNTs in previous studies [2,29,31]. The similar anisotropy could explain the relatively low thermal conductivity in this work, which is that each fiber in the CNF consists of the graphitic structure and the fibers are intertwined to form one CNF (Fig. 2). The CNF was bridged on the hot film and sensor, and amorphous carbon was deposited on the both contacts to minimize the thermal contact resistances. Heat was transported from the hot film into the CNF through the outer part of the CNF where the CNF is on the hot film and/or is connected to the hot film by covering with the amorphous carbon deposition. Because of the anisotropic structure of the CNF, heat is likely to be transported in the fiber-axis direction, resulting in that fibers and graphene layers closer to the bottom side and/or the outer surface contribute more largely to the thermal transport. The relatively low effective thermal conductivity was calculated from the thermal resistance using the whole cross-sectional area.

The decrease of the thermal conductivity after the first FIB irradiation is much smaller than that previously reported for graphene-based nanocarbon materials. For example, amorphization of a part of the MWCNT by FIB irradiation led to a 41% decrease in the thermal conductance of the MWCNT [10]. In addition, the introduction of nanohole defects by FIB irradiation led to a decrease of the thermal conductivity of SLG by 42% [11]. Some theoretical studies have also reported that the introduction of a small number of vacancy defects can largely decrease the thermal conductivities of SWCNTs [32] and SLG [12,33]. The difference between the previous and current results could arise from the difference in the structures. The CNT and graphene essentially consist of SLG, where the defects disturb phonon propagation in each graphene layer. In contrast, the CNF consists of many individual fibers made of multi-layer graphene. In this study, the fibers in the 46% of the cross-section were estimated to be crystalline after the FIB irradiation. Especially, the remaining crystalline fibers are in the roughly lower half of the CNF which largely contributed to the thermal transport in the CNF since the crystalline fibers are close to the hot film. It should be noted that there was still room for the thermal conductivity of the pristine CNF to decrease because it is higher than that of amorphous carbon [34] where the structure is disordered and whose thermal conductivity is the lower limit (Fig. S10).

The results in Fig. 5 were analyzed using a thermal-circuit model consisting of the thermal resistances of the CNF divided by the defected parts. The model is shown in Fig. 6. $R_{n\mathrm{th}}$ is the measured thermal resistance of the CNF after the nth FIB irradiation (n=0, 1, 2, 3, 4). L_i, k_i and R_i correspond to the length, thermal conductivity, and thermal resistance of the ith pristine part of the CNF (i=1, 2, 3, 4, 5). After the first FIB irradiation, a defected part was created in the CNF because of the local amorphization of the CNF, and the CNF was divided into three different-length parts of L_1 (0.822 μm), L_d (0.222 μm), and L_4 (3.956 μm). L_d is the length of the defected part. The total thermal resistance of the CNF can be expressed as

$$R_{1\mathrm{st}}=R_1+R_\mathrm{d}+R_4. \quad (1)$$

Similarly, after the nth FIB irradiation, n defected parts were created in the CNF, and the total thermal resistance of the CNF can be expressed as

$$R_{n\mathrm{th}}=n(R_1+R_\mathrm{d})+R_{5-n}. \quad (2)$$

All the R_d values were assumed to be identical.

To solve the equations, we assumed two cases in which the length was longer than ~4 μm. In the first case, we used assumption (i) of diffusive phonon transport (k_4=k_5). If this assumption is valid, the thermal conductivities k_i (i=1, 2, 3, 4, 5) should not change. Under assumption (i), R_1+R_d was determined using equation (1), and R_{5-n} was finally derived from equation (2). The k_{5-n} values converted from R_{5-n} are presented in Fig. 7 as a function of the characteristic length L_{5-n} as solid blue squares. However, the resultant thermal conductivity decreased with decreasing characteristic length, which implies that thermal transport in the CNF included the ballistic feature of phonons. Next, assumption (ii) of quasi-ballistic phonon transport ($k_4=\alpha L_4^{\beta}$) was adopted. It has been theoretically predicted and experimentally demonstrated that the thermal conductivities of one-dimensional materials diverge as $\sim L^{\beta}$ (β is between 0 and 1) [17,35,36]. For our assumption (ii), β was estimated to be 0.023 in accordance with ref. [17], where the thermal conductivity of a SWCNT was reported to diverge as $\sim L^{\beta}$ (β=0.023, 3.0 μm<L<5.5 μm). α was determined to be 654 from the thermal conductivity k_5 ($k_5=\alpha L_5^{0.023}$). The resultant thermal conductivities are plotted as a function of characteristic length in Fig. 7 as open blue squares. In Fig. 7, both the thermal conductivities obtained using assumption (i) and (ii) respectively decreased as the characteristic length of the CNF decreased in the micrometer range. The thermal conductivity (assumption (i)) shows that the thermal transport in the CNF is not completely diffusive, and the thermal conductivity (assumption (ii)) suggests how it could depend on the characteristic length.

This finding, that the thermal conductivity of the CNF could depend on the characteristic length in the micrometer range, is similar to the experimentally reported size effects for SWCNTs, SLG, and MWCNTs. The thermal conductivities of SWCNTs were observed to saturate to finite values at a characteristic length of ~10 μm [17]. In addition, the thermal conductivity of SLG has been shown to logarithmically increase in the length range from 300 nm to 9 μm [37]. For MWCNTs, Chang et al. reported the violation of Fourier's law in the length range of 3.7–5.4 μm [38]. In addition, Hayashi and co-authors reported that the thermal conductivity of MWCNTs monotonically increase in the length range of 0.3–4.8 μm [10]. These length dependences of the thermal conductivities exist over a longer regime than the roughly estimated phonon mean free paths of SWCNTs (250–750 nm) [29], SLG (240–775 nm) [6,37], and MWCNTs (4–50 nm) [4,27] near room temperature. However, these phonon mean free paths were determined using a simple kinetic theory that ignored phonon dispersion. In fact, there are phonons with various mean free paths, and the phonons with long mean free paths could largely contribute to thermal transport [10,39]. The phonons with long mean free paths produced by graphene-based structures in SWCNTs, SLG, and MWCNTs contribute largely to their thermal transport, leading to the remaining feature of ballistic phonon transport and length-dependent thermal conductivity in the micrometer range. Here, the length-dependent thermal conductivity of the CNF can be attributed to the fibers made of the graphitic structure which can continue for a long distance. It was observed that the graphitic structures were oriented with respect to the axis of the CNF to some extent and continued essentially in the axial direction of the CNF. As far as we observed, there was no cuts of the fibers while some fibers could not be observed due to going beneath others and/or being twisted. The graphitization at 2800 °C contributed to creating the long-continuing structure and helped the ballistic feature of the phonons to remain in the micrometer range, leading to this anomalous characteristic of the CNF such as for CNTs and graphene. Previous studies have also reported that such graphene-based structures lead to ballistic phonon transport even for effective thermal conductivities of 10–100 W/mK [18,23,40].

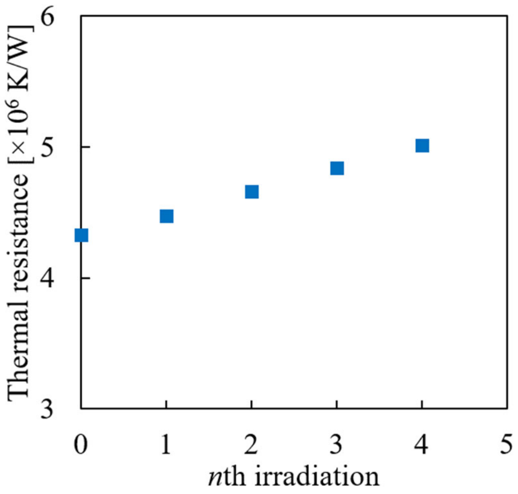

Fig. 5. Thermal resistance of CNF after *n*th irradiation.

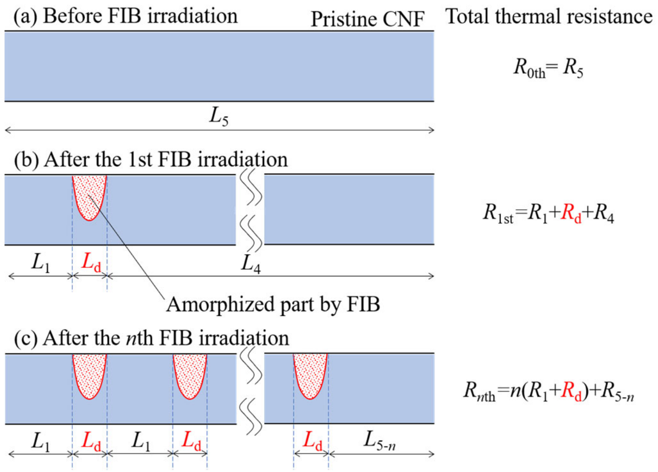

Fig. 6. Schematic illustration of thermal-circuit model of CNF. (a) Before FIB irradiation, the

total thermal resistance of the CNF was $R_{0\mathrm{th}}$. (b) After the first FIB irradiation, the CNF was divided into three different-lengths parts L_1, L_d, and L_4. The total thermal resistance of the CNF can be expressed as $R_{1\mathrm{st}}=R_1+R_\mathrm{d}+R_4$. (c) Similarly, after the *n*th FIB irradiation, the total thermal resistance of the CNF can be expressed as $R_{n\mathrm{th}}=n(R_1+R_\mathrm{d})+R_{5-n}$.

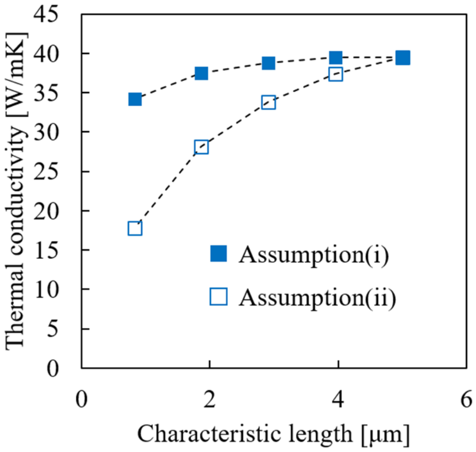

Fig. 7. Thermal conductivities of CNF obtained under assumption (i) (solid blue squares) of diffusive phonon transport and assumption (ii) (open blue squares) of quasi-ballistic phonon transport as a function of characteristic length. The dashed lines were drawn to guide the eyes.

4. Conclusions

We investigated thermal transport in a CNF using a T-type thermal merereurement method with a Pt hot-film sensor and FIB nanofabrication. TEM analysis revealed that the FIB irradiations on the CNF amorphized the crystalline structure. In addition, correction of the effect of scattered ions on the Pt hot film led to more precise in situ measurements. The relatively low thermal conductivity resulted from the anisotropic fibrous structure. The measured thermal resistance of the CNF increased with increasing irradiation time. Compared with the results of previous studies, the decrease in the thermal conductivity was small after the first FIB irradiation as some fibers remained pristine even after the FIB irradiation. Analysis using a thermal-circuit model suggests that there could be a length-dependent thermal conductivity of the CNF with a characteristic length ranging from ~1 to ~5 μm. Our proposed experimental approach can also be applied to in situ thermal and/or electrical measurements of other nanomaterials while modifying their structure.

Acknowledgements

This work was partially supported by JSPS KAKENHI (Grant Nos. JP17H03186 and JP18K13704), JST CREST Grant No. JPMJCR18I1, and a Grant-in-Aid for JSPS Research Fellow No. JP18J11632. The TEM observations were performed at the Ultramicroscopy Research Center at Kyushu University.

References

[1] P. Kim, L. Shi, A. Majumdar, P.L. McEuen, Thermal Transport Measurements of Individual Multiwalled Nanotubes, Phys. Rev. Lett. 87 (2001) 215502.

doi:10.1103/PhysRevLett.87.215502.

[2] M. Fujii, X. Zhang, H. Xie, H. Ago, K. Takahashi, T. Ikuta, H. Abe, T. Shimizu, Measuring the Thermal Conductivity of a Single Carbon Nanotube, Phys. Rev. Lett. 95 (2005) 065502. doi:10.1103/PhysRevLett.95.065502.

[3] C. Yu, L. Shi, Z. Yao, D. Li, A. Majumdar, Thermal Conductance and Thermopower of an Individual Single-Wall Carbon Nanotube, Nano Lett. 5 (2005) 1842–1846. doi:10.1021/nl051044e.

[4] T.-Y. Choi, D. Poulikakos, J. Tharian, U. Sennhauser, Measurement of the Thermal Conductivity of Individual Carbon Nanotubes by the Four-Point Three-ω Method, Nano Lett. 6 (2006) 1589–1593. doi:10.1021/nl060331v.

[5] A.A. Balandin, S. Ghosh, W. Bao, I. Calizo, D. Teweldebrhan, F. Miao, C.N. Lau, Superior Thermal Conductivity of Single-Layer Graphene, Nano Lett. 8 (2008) 902–907. doi:10.1021/nl0731872.

[6] S. Ghosh, I. Calizo, D. Teweldebrhan, E.P. Pokatilov, D.L. Nika, A.A. Balandin, W. Bao, F. Miao, C.N. Lau, Extremely high thermal conductivity of graphene: Prospects for thermal management applications in nanoelectronic circuits, Appl. Phys. Lett. 92 (2008) 151911. doi:10.1063/1.2907977.

[7] M.J. Biercuk, M.C. Llaguno, M. Radosavljevic, J.K. Hyun, A.T. Johnson, J.E. Fischer, Carbon nanotube composites for thermal management, Appl. Phys. Lett. 80 (2002) 2767–2769. doi:10.1063/1.1469696.

[8] W. Jiang, G. Ding, H. Peng, Measurement and model on thermal conductivities of carbon nanotube nanorefrigerants, Int. J. Therm. Sci. 48 (2009) 1108–1115. doi:10.1016/j.ijthermalsci.2008.11.012.

[9] A.M. Marconnet, N. Yamamoto, M.A. Panzer, B.L. Wardle, K.E. Goodson, Thermal Conduction in Aligned Carbon Nanotube–Polymer Nanocomposites with High Packing Density, ACS Nano. 5 (2011) 4818–4825. doi:10.1021/nn200847u.

[10] H. Hayashi, K. Takahashi, T. Ikuta, T. Nishiyama, Y. Takata, X. Zhang, Direct evaluation of ballistic phonon transport in a multi-walled carbon nanotube, Appl. Phys. Lett. 104 (2014) 113112. doi:10.1063/1.4869470.

[11] H. Wang, K. Kurata, T. Fukunaga, H. Takamatsu, X. Zhang, T. Ikuta, K. Takahashi, T. Nishiyama, H. Ago, Y. Takata, In-situ measurement of the heat transport in defect-engineered free-standing single-layer graphene, Sci. Rep. 6 (2016) 21823. doi:10.1038/srep21823.

[12] H. Malekpour, P. Ramnani, S. Srinivasan, G. Balasubramanian, D.L. Nika, A. Mulchandani, R.K. Lake, A.A. Balandin, Thermal conductivity of graphene with

defects induced by electron beam irradiation, Nanoscale. 8 (2016) 14608–14616. doi:10.1039/C6NR03470E.

[13] H. Wang, S. Hu, K. Takahashi, X. Zhang, H. Takamatsu, J. Chen, Experimental study of thermal rectification in suspended monolayer graphene, Nat. Commun. 8 (2017) 15843. doi:10.1038/ncomms15843.

[14] T. Kodama, M. Ohnishi, W. Park, T. Shiga, J. Park, T. Shimada, H. Shinohara, J. Shiomi, K.E. Goodson, Modulation of thermal and thermoelectric transport in individual carbon nanotubes by fullerene encapsulation, Nat. Mater. 16 (2017) 892–897. doi:10.1038/nmat4946.

[15] W. Zhao, Y. Wang, Z. Wu, W. Wang, K. Bi, Z. Liang, J. Yang, Y. Chen, Z. Xu, Z. Ni, Defect-Engineered Heat Transport in Graphene: A Route to High Efficient Thermal Rectification, Sci. Rep. 5 (2015) 11962. doi:10.1038/srep11962.

[16] M. Narasaki, H. Wang, T. Nishiyama, T. Ikuta, K. Takahashi, Experimental study on thermal conductivity of free-standing fluorinated single-layer graphene, Appl. Phys. Lett. 111 (2017) 093103. doi:10.1063/1.5001169.

[17] J. Liu, T. Li, Y. Hu, X. Zhang, Benchmark study of the length dependent thermal conductivity of individual suspended, pristine SWCNTs, Nanoscale. 9 (2017) 1496–1501. doi:10.1039/C6NR06901K.

[18] Y. Yamada, A. Askounis, T. Ikuta, K. Takahashi, Y. Takata, K. Sefiane, Thermal conductivity of liquid/carbon nanotube core-shell nanocomposites, J. Appl. Phys. 121 (2017) 015104. doi:10.1063/1.4973488.

[19] N.F.W. Thissen, R.H.J. Vervuurt, J.J.L. Mulders, J.W. Weber, W.M.M. Kessels, A.A. Bol, The effect of residual gas scattering on Ga ion beam patterning of graphene, Appl. Phys. Lett. 107 (2015) 213101. doi:10.1063/1.4936334.

[20] Z. Liao, T. Zhang, M. Gall, A. Dianat, R. Rosenkranz, R. Jordan, G. Cuniberti, E. Zschech, Lateral damage in graphene carved by high energy focused gallium ion beams, Appl. Phys. Lett. 107 (2015) 013108. doi:10.1063/1.4926647.

[21] M. Narasaki, H. Wang, Y. Takata, K. Takahashi, Influence of ion beam scattering on the electrical resistivity of platinum hot films, Microelectron. Eng. 166 (2016) 15–18. doi:10.1016/j.mee.2016.09.008.

[22] L. Shi, D. Li, C. Yu, W. Jang, D. Kim, Z. Yao, P. Kim, A. Majumdar, Measuring Thermal and Thermoelectric Properties of One-Dimensional Nanostructures Using a Microfabricated Device, J. Heat Transfer. 125 (2003) 881. doi:10.1115/1.1597619.

[23] A. Askounis, Y. Yamada, T. Ikuta, K. Takahashi, Y. Takata, K. Sefiane, On the linear dependence of a carbon nanofiber thermal conductivity on wall thickness, AIP Adv. 6 (2016) 115119. doi:10.1063/1.4968831.

[24] Z. Zhou, C. Lai, L. Zhang, Y. Qian, H. Hou, D.H. Reneker, H. Fong, Development of carbon nanofibers from aligned electrospun polyacrylonitrile nanofiber bundles and characterization of their microstructural, electrical, and mechanical properties, Polymer (Guildf). 50 (2009) 2999–3006. doi:10.1016/j.polymer.2009.04.058.

[25] E. Pop, D. Mann, Q. Wang, K. Goodson, H. Dai, Thermal Conductance of an Individual Single-Wall Carbon Nanotube above Room Temperature, Nano Lett. 6 (2006) 96–100. doi:10.1021/nl052145f.

[26] Q. Li, C. Liu, X. Wang, S. Fan, Measuring the thermal conductivity of individual carbon nanotubes by the Raman shift method, Nanotechnology. 20 (2009) 145702. doi:10.1088/0957-4484/20/14/145702.

[27] M.T. Pettes, L. Shi, Thermal and Structural Characterizations of Individual Single-, Double-, and Multi-Walled Carbon Nanotubes, Adv. Funct. Mater. 19 (2009) 3918–3925. doi:10.1002/adfm.200900932.

[28] T.Y. Choi, D. Poulikakos, J. Tharian, U. Sennhauser, Measurement of thermal conductivity of individual multiwalled carbon nanotubes by the 3-ω method, Appl. Phys. Lett. 87 (2005) 013108. doi:10.1063/1.1957118.

[29] J. Yang, S. Waltermire, Y. Chen, A.A. Zinn, T.T. Xu, D. Li, Contact thermal resistance between individual multiwall carbon nanotubes, Appl. Phys. Lett. 96 (2010)

023109. doi:10.1063/1.3292203.

[30] J. Yang, Y. Yang, S.W. Waltermire, T. Gutu, A.A. Zinn, T.T. Xu, Y. Chen, D. Li, Measurement of the Intrinsic Thermal Conductivity of a Multiwalled Carbon Nanotube and Its Contact Thermal Resistance with the Substrate, Small. 7 (2011) 2334–2340. doi:10.1002/smll.201100429.

[31] H. Hayashi, T. Ikuta, T. Nishiyama, K. Takahashi, Enhanced anisotropic heat conduction in multi-walled carbon nanotubes, J. Appl. Phys. 113 (2013) 014301. doi:10.1063/1.4772612.

[32] C. Sevik, H. Sevinçli, G. Cuniberti, T. Çağın, Phonon Engineering in Carbon Nanotubes by Controlling Defect Concentration, Nano Lett. 11 (2011) 4971–4977. doi:10.1021/nl2029333.

[33] T. Feng, X. Ruan, Z. Ye, B. Cao, Spectral phonon mean free path and thermal conductivity accumulation in defected graphene: The effects of defect type and concentration, Phys. Rev. B. 91 (2015) 224301. doi:10.1103/PhysRevB.91.224301.

[34] C.Y. Ho, R.W. Powell, P.E. Liley, Thermal Conductivity of the Elements, J. Phys. Chem. Ref. Data. 1 (1972) 279–421. doi:10.1063/1.3253100.

[35] B. Li, J. Wang, Anomalous Heat Conduction and Anomalous Diffusion in

One-Dimensional Systems, Phys. Rev. Lett. 91 (2003) 044301. doi:10.1103/PhysRevLett.91.044301.

[36] A. Dhar, Heat transport in low-dimensional systems, Adv. Phys. 57 (2008) 457–537. doi:10.1080/00018730802538522.

[37] X. Xu, L.F.C. Pereira, Y. Wang, J. Wu, K. Zhang, X. Zhao, S. Bae, C. Tinh Bui, R. Xie, J.T.L. Thong, B.H. Hong, K.P. Loh, D. Donadio, B. Li, B. Özyilmaz, Length-dependent thermal conductivity in suspended single-layer graphene, Nat. Commun. 5 (2014) 3689. doi:10.1038/ncomms4689.

[38] C.W. Chang, D. Okawa, H. Garcia, A. Majumdar, A. Zettl, Breakdown of Fourier's Law in Nanotube Thermal Conductors, Phys. Rev. Lett. 101 (2008) 075903. doi:10.1103/PhysRevLett.101.075903.

[39] K.T. Regner, D.P. Sellan, Z. Su, C.H. Amon, A.J.H. McGaughey, J.A. Malen, Broadband phonon mean free path contributions to thermal conductivity measured using frequency domain thermoreflectance, Nat. Commun. 4 (2013) 1640. doi:10.1038/ncomms2630.

[40] K. Takahashi, Y. Ito, T. Ikuta, X. Zhang, M. Fujii, Experimental and numerical studies on ballistic phonon transport of cup-stacked carbon nanofiber, Phys. B Condens. Matter. 404 (2009) 2431–2434. doi:10.1016/j.physb.2009.05.001.